Available online at www.sciencedirect.com
SCIENCE DIRECT
Journal of Colloid and Interface Science 294 (2006) 436–448
JOURNAL OF Colloid and Interface Science
www.elsevier.com/locate/jcis

Force balance conditions for droplet formation in cross-flow membrane emulsifications

G. De Luca *, E. Drioli

Institute on Membrane Technology (ITM-CNR), c/o University of Calabria, Via P. Bucci 17/C, 87030 Rende (CS), Italy

Received 29 April 2005; accepted 23 July 2005
Available online 31 August 2005

Abstract

The membrane emulsification process is becoming of growing interest in many industrial fields. For monitoring the influence of process and membrane parameters on the droplet formation, quantitative information on the droplet detachment, during this process, is important. Until now, droplet formation has theoretically been described using computational fluid dynamics and global force equations. Unlike computational fluid dynamics methods, the global force models are less accurate but easier to handle and instructive. On this basis, in the present paper we present new force balance equations to describe droplet detachment during cross-flow membrane emulsification. In a first approximation, the droplet is supposed to grow leaning on the pore border as long as a force balance exists along the contact line located on the membrane surface. During this phase the base of the droplet, still stuck on the pore border, begins to bend on the membrane surface until its final detachment. Using force balance equations made along the contact lines, we obtain the minimum and maximum sizes that a droplet could have during cross-flow membrane emulsification. This approach is tested with different continuous phase velocities, membrane pore sizes and interfacial tensions. The results are compared to various experimental data, reported in literature. In particular, based on the experimentally found linear correlation between droplet and pore sizes, we show how the proposed balance equations can be used to obtain a satisfactory evaluation of the slopes of this linear correlation and how these force balances could be used to obtain an estimation of the interfacial tensions during the droplet formation.

Keywords: Cross-flow membrane emulsification; Force balance; Contact lines; Advancing and receding contact angles; Mean droplet sizes; Interfacial tensions; Droplet formation mechanisms

1. Introduction

For large-scale emulsion productions, the most employed methods are based on the establishment of turbulent flows in the fluid mixtures. Recently, more attention has been addressed to an alternative emulsification process, i.e., the cross-flow membrane emulsification. Cross-flow membrane emulsification is a relatively new membrane technology [1], which allows the emulsion production in which the droplet sizes are obtained under controlled conditions. In this procedure both droplet sizes and size distributions may be carefully and easily controlled choosing suitable membranes and process parameters. This feature is very important, since the emulsion stability and its properties are determined by the droplet size and size distribution. Cross-flow membrane emulsification is also an efficient process, since the energy density requirement (energy input per cubic meter of emulsion produced) is low with respect to the other emulsification techniques [2]; especially for emulsions with droplet sizes smaller than 1 μm. Furthermore, this lower energy density requirement improves the quality and functionality of delicate emulsion ingredients. In fact, in the conventional emulsification methods the high shear rate and consequent increase of the process temperature has negative effects on the most delicate emulsion components.

Membrane emulsifications can be distinguished in: (i) pre-mix membrane emulsification, in which a coarse pre-

* Corresponding author. Fax: +39 0984 402103.
E-mail address: g.deluca@itm.cnr.it (G. De Luca).

0021-9797/$ – see front matter
doi:10.1016/j.jcis.2005.07.055

mixed emulsion is pressed through the membrane pores to reduce the droplet sizes, and (ii) cross-flow membrane emulsification in which the disperse phase (e.g., oil) is directly pressed through the membrane pores to obtain droplets. In a Cross-flow Membrane Emulsification (CME), the droplets, formed at the pore mouth, grow until a critical dimension; then they are carried away with the continuous phase (e.g., water), flowing parallel to the membrane surface. However, emulsions with droplet diameters above 0.1 μm, generally require some additional substances, i.e., emulsifiers or stabilizers, to protect the droplets against coalescence.

The droplet size in a CME depends on several parameters, as shown in different works [2–5]. Among these, the most important are: (i) trans-membrane pressure, (ii) continuous phase cross-flow velocity, (iii) membrane pore size and morphology, (iv) hydrophobicity or hydrophilicity of the membrane surface, (v) dynamic interfacial tension. Concerning the influence of these parameters, it is important to note that in a CME, a linear correlation between droplet sizes and membrane pore diameters has experimentally been established [4,6,7]; therefore the cited quantities explicitly affect the slope of this linear correlation.

From a theoretical point of view, the cross-flow membrane emulsification processes have been analysed using two different approaches: (i) computational fluid dynamics [2,8] and (ii) force balance equations [9–12]. Although recognizing the existence of droplet deformations from a spherical shape during its formation, the works based on force balance equations do not take into account these deformations. Furthermore, the forces evoked in these studies have always been used to correlate the droplet sizes with cross-flow velocities [9] or with continuous phase viscosity [12], but never with the membrane pore sizes [13].

Consequently, in this work we have analysed the experimental linear correlation between droplet size and membrane pore diameters by using new force balance equations (not employed in the quoted works). The proposed force balance takes into account the droplet deformation occurring at the droplet base, calculating the advancing and receding contact angles during the droplet formation. It is important to note that in our approach the drag force due to cross-flow continuous velocity is considered as the driving force of droplet (de) formation. Droplets formed without continuous phase flow, where the disperse phase is spontaneously transformed into spherical droplets [14,15], is not considered here. The spontaneous transformation model explains the experimental results (droplet sizes) at low disperse phase flux and at zero or low continuous phase flow velocity [15,16].

Concerning the force balance approaches, it is important to underline the limits beyond which these equations could not be valid. In particular, a fluid that flows through the membrane pores can be considered as continuous when the mean free path of its molecules is smaller than the membrane pore diameters. This condition is generally true for liquids that flow in pores with diameters of hundreds of nano-meters, since the main free path of their molecules is in the order of few Ångströms. Nevertheless, attention must be paid to force expressions used in these balance equations. In fact, although in the micro-pores a liquid behaves as a continuous medium, for these dimensions the macroscopic force expressions could be not valid; e.g., a nano-pore could contain a limited number of molecules and therefore fluctuations of the average macroscopic forces could occur.

To summarise, in this paper we analyse the linear correlation, experimentally found during a CME process, between droplet and membrane pore diameters by using new force balance equations which take into account the deformations that occur at the base of droplet (advancing and receding contact angles). We investigate, also, the influence of the cross-flow velocity and interfacial tension on droplet sizes, during a CME.

2. Theoretical method

In this work, we suppose that distortions occur at the base of droplet, stuck on the pore border. The contact line on the membrane surface, which can depend on the form of the membrane pore border, defines the base of the droplet. We show how a force balance along this contact line yields a relation between the droplet diameters and the advancing and receding contact angles (Fig. 1) along the contact line. It is important to note that the considered advancing and receding contact angles define the limits of the values that the contact angle along the contact line can assume.

This approach supposes that the shape of the contact line is known a priori. However, for symmetric shapes, as shown in Fig. 2a (slot shape), the width of the contact line can be considered as the most relevant dimension. Concerning this point, in our calculations we consider both slot and circular contact lines, as reported in Fig. 2. We assume that the width of the contact line (longer length), having slot shape, is equal to the membrane pore size, whereas the side lines (bc) are considered small with respect to the advancing and receding portions (Fig. 2). In the case of a circular contact line, the arcs (bc) are considered small compared to the complete circumference, having a diameter equal to the pore size.

Although we consider these constraints on contact line shapes, the following force balance equations are valid for any contact line. Precisely, the sum of forces acting on a droplet, stuck on a general contact line, yields:

$$\begin{cases} \int_l \gamma\big(\bar{M}(D_{\text{droplet}})\cdot\bar{m}\big)\bar{m}\,\mathrm{d}l + F_{\text{DR}}(D_{\text{droplet}})i = 0, \\ \int_l \gamma\sin(\theta)k\,\mathrm{d}l + \big[F_{\text{YL}}(D_{\text{droplet}}) + F_{\text{DL}}(D_{\text{droplet}}) \\ \quad + F_{\text{BG}}(D_{\text{droplet}})\big]k = 0, \end{cases} \tag{1}$$

where l depends on the shape of the contact line, **M** and **m** are the unit vectors, whose directions are indicated in Figs. 1 and 2, respectively, moreover we make use of the following

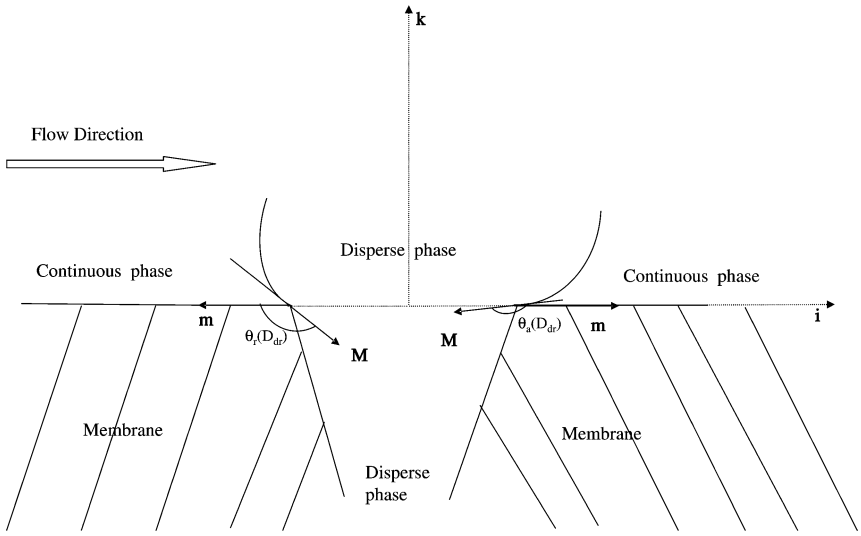

Fig. 1. Advancing and receding contact angles in the schematic representation of the droplet base. Unit vector directions (**M**, **m**) respect to membrane surface.

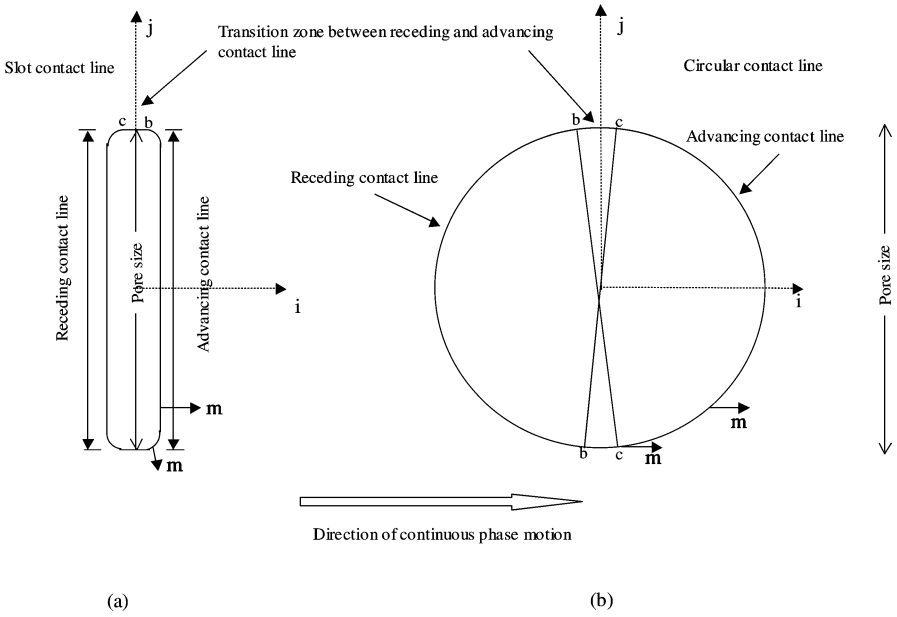

Fig. 2. Schematic representation of contact line (top view) for a slot shape (a) and a circular shape (b) forming the droplet basis.

definition of the contact angle:

$$\bar{M}(D_{\text{droplet}}) \cdot \bar{m} = \cos\theta. \tag{2}$$

The quantity γ represents the interfacial tension of the oil/water interface, containing a certain concentration of emulsifier; here we consider only the tension along the contact line oil/water. The integration along the considered contact lines can be divided into four segments: the advancing (l_a) and receding (l_r) portions, along which the contact angles assume the constant values of θ_a and θ_r, respectively, and the two lines on the sides of the droplet (bc) (Fig. 2) in which the contact angles are not constant. Upon the integration along the advancing (l_a), receding (l_r) and side portions, owing to the contact line symmetry the total $\bar{m} \cdot j$ component of integration must be zero, hence Eq. (1) can be rewritten as:

$$\begin{cases} \gamma\cos\theta_a \int_{l_a} \bar{m}\cdot i\,\mathrm{d}l + \gamma\cos\theta_r \int_{l_r} \bar{m}\cdot i\,\mathrm{d}l \\ \quad + 2\gamma \int_{bc} \cos\theta(l)\bar{m}\cdot i\,\mathrm{d}l + F_{DR}(D_{\text{droplet}}) = 0, \\ \gamma\sin\theta_a \int_{l_a} k\cdot k\,\mathrm{d}l + \gamma\sin\theta_r \int_{l_r} k\cdot k\,\mathrm{d}l \\ \quad + 2\gamma \int_{bc} \sin\theta(l) k\cdot k\,\mathrm{d}l + \big[F_{YL}(D_{\text{droplet}}) \\ \quad + F_{DL}(D_{\text{droplet}}) + F_{BG}(D_{\text{droplet}})\big] = 0. \end{cases} \tag{3}$$

Eq. (3) are valid for any j-symmetric contact line. However, before considering particular shapes of contact line, the validation of the proposed approach is necessary. Therefore, we have used Eq. (3) with slot and circular shaped contact lines (see Appendix A) in the interpretation of some important experimental trends, found in the cross-flow membrane emulsifications.

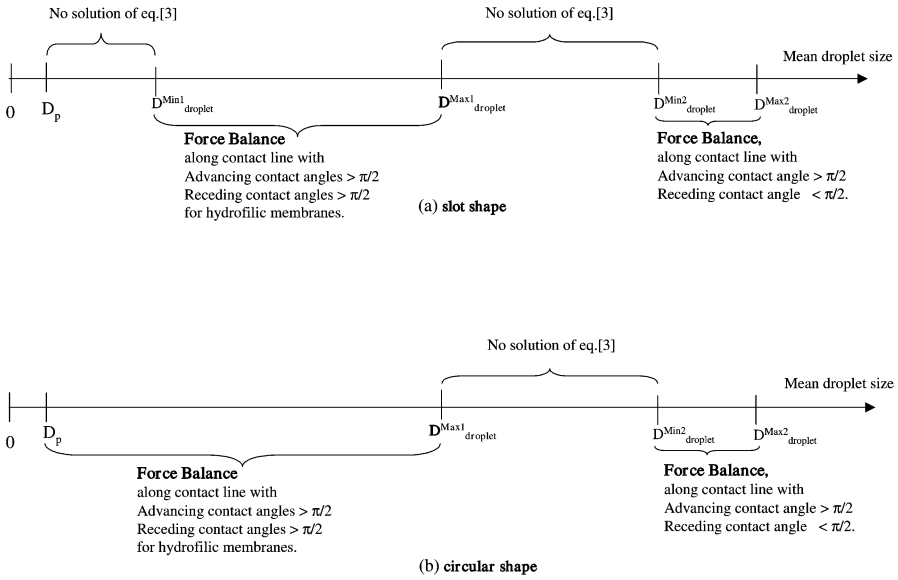

Fig. 3. Solution ranges for the droplet size according to Eq. (3) for a contact line having a slot shape and pore sizes below 8 μm (a) and for a circular contact line (b).

The forces considered in Eq. (3) and perpendicular to membrane surface are the static pressure difference force F_{YL} [11,12], the dynamic lift and buoyancy forces (F_{DL}, F_{BG}) [9,12] defined as:

$$F_{YL} = \frac{\gamma}{\langle D_{droplet}\rangle}\pi D_p^2, \tag{4}$$

$$F_{DL} = 0.761\frac{\tau_{c,s}^{1.5}\rho_c^{0.5}}{\mu_c}\langle D_{droplet}\rangle^3, \tag{5}$$

$$F_{BG} = \frac{1}{6}\pi g \Delta\rho \langle D_{droplet}\rangle^3. \tag{6}$$

The drag force (F_{DR}) [9,11,12] due to continuous cross-flow and parallel to membrane surface is defined by means of Stokes equation [9]:

$$F_{DR} = \frac{3}{2}k_x \pi \tau_{c,s}\langle D_{droplet}\rangle^2. \tag{7}$$

The k_x parameter in Eq. (7), is equal to 1.7 and takes into account the wall correction factor for a single sphere touching an impermeable wall [17]. Finally, D_p in Eq. (4) corresponds to the average membrane pore size, while $\tau_{c,s}$, ρ_c and μ_c, in Eqs. (5) and (7), represent the wall shear stress, the density and viscosity of the continuous phase, respectively. The quantity, $\Delta\rho$, in Eq. (6) corresponds to the difference between continuous and disperse phase density. In the Stokes equation (7) the following approximation $v_{c,c}^{\infty}\mu_c \approx 1/2\tau_{c,s}\langle D_{droplet}\rangle$ was adopted, in which we assume that the shear stress at the droplet centre is equal to the shear stress at the membrane surface, i.e., $\tau_{c,s}$.

The effective pressure ΔP_{eff}, during an emulsification process, is defined as the difference between the applied trans-membrane and Young–Laplace pressure [11]. The effective pressure determines the phase disperse flux through the membrane pores $J_d(\Delta P_{eff})$. It presents a minimum when Young–Laplace pressure is equal to critical pressure. Therefore, in steady condition, the disperse phase unloads its momentum on the droplet, i.e., the linear momentum force [11]. This force depends on the J_d (ΔP_{eff}), as well as on the applied trans-membrane pressure. The linear momentum force can be neglected for trans-membrane pressures slightly higher than critical pressure (low phase disperse flux). Although, the experimental data analysed in this work are obtained with trans-membrane pressures slightly higher than critical pressure, the presented method also permits to take into account the linear momentum force introducing this force in the balance equation (1).

The interfacial tension in Eqs. (1), (3) and (4) is the same because we consider droplet contact line (oil/water) having a small thickness.

Therefore, its upper part permits the droplet to stick on the pore border. This approach has already been used to describe a droplet stuck on non-horizontal surfaces of solids [18] and in several works on membrane emulsifications [11, 12]. However, in the proposed method, according to membrane hydrophilicity it is possible to define two different interfacial tensions: the first in the integral calculus of Eqs. (1) and (3), the second in Eq. (4). The first tension takes into account the interaction between oil/water interface and membrane surface, the second considers only the oil/water interfacial tension.

It is important to stress that the average droplet diameter $\langle D_{droplet}\rangle$, in Eq. (3), yields an estimation of the largest droplet volume that could be formed. In fact, it is well known [8] that a fraction of this largest volume remains attached at the pore border. The simulations of Gijsbertsen-Abrahamse et al. [8] clearly slow (see Fig. 3 of the paper) that the droplet, stuck at the membrane surface, reaches a definite volume, after which a necking at the droplet base begins, causing the final droplet formation. Thus, when a droplet

Table 1
Minimum and Maximum (Max1 and Max2) droplet diameters according to balance equation (3) using a slot shaped contact line and mean pore sizes ranging from 0.5 to 10.0 μm. The employed interfacial tension and cross-flow velocity are equal to 7 mN/m and 1.4 m/s, respectively. The droplet size step used in the calculations is 0.1 μm

Mean pore size, D_p (μm)	$\langle D^{Min1}_{droplet}\rangle$ (μm)	$\langle D^{Max1}_{droplet}\rangle$ (μm)	$\langle D^{Max2}_{droplet}\rangle$ (μm)	$(D^{Max1}_{droplet}/D_p)$[a]	$D^{Max2}_{droplet}/D_p$
0.5	0.7	2.8	10.9	5.60	21.80
1.0	1.4	4.8	15.4	4.80	15.40
2.0	2.8	8.3	21.6	4.15	10.80
5.0	7.2	17.5	33.1	3.50	6.62
6.0	8.4	20.4	35.9	3.40	5.98
8.0	11.2	–	40.7	1.40	5.09
10.0	14.5	–	44.5	1.45	4.45

[a] For last two pore sizes the solution sets are continuous, while for all pore sizes $(D^{Min1}_{droplet}/D_p)$ is 1.4.

necking is formed outside the pore, the size of final droplet will be always smaller than the volume corresponding to the average diameter $\langle D_{droplet}\rangle$. The location of droplet necking (outside or inside the pore) depends on the pore shape. However, the reported observations on the location of droplet necking inside the pore refer to droplets formed using very low cross-flow velocity [19]. Therefore, in this work the above assumption on average droplet diameter can be considered.

3. Results and discussion

In this section, we present the comparison between the results obtained from Eq. (3) and experimental data available in the literature. Katoh et al. [6] and Vladisavljevic and Schubert [7] have reported different data on oil/water emulsions, obtained with tubular hydrophilic Shirasu-porous-glass (SPG) membranes. These data are suitable for a theoretical interpretation, because:

(i) structural modifications (i.e., hydrophilic and hydrophobic modifications), due to the membrane pre-treatment, are completely absent. Membrane pre-treatments have not been necessary in these experiments;
(ii) in these experiments the conditions for unhindered droplet growth are satisfied;
(iii) complete experimental data, i.e., capillary pressures, average droplet sizes, droplet formation times, membrane pore sizes and average cross-flow velocities have been given;
(iv) membrane module dimensions are reported.

Using the SPG membrane with a mean pore diameter of 15 μm, Yasuno et al. [15] have shown that when the disperse-phase flux was below 2×10^{-6} m^3/(m^2 s) and the continuous-phase flow velocity was above 0.3 m/s, both the shear force and spontaneous formation mechanisms play a large role in the droplet detachment. In the experiments of Katoh et al. [6] and Vladisavljevic and Schubert [7], the disperse-phase fluxes are similar to the previous one, while the cross-flow velocities are markedly higher, therefore a shear force mechanism is applicable to the interpretation of these data. However, we are aware that the shapes of the contact lines used in our calculations could be too simple to represent the real contact lines (similar to pore border) in these cases, but it is important to stress that the droplet contact line is not necessarily equal to the pore border.

Kobayashi et al. [20] have reported the real-time microscopic observations of the droplet formation on a flat rectangular-type hydrophilic polycarbonate membrane with a mean pore size of 10 μm. Similar to the previous experimental works, the data of Kobayashi et al. [20] are in accordance with the approximations of proposed method. Moreover, Kobayashi et al. describe in their work the influence of the continuous phase flow velocity and the surfactant types on the droplet diameters.

Before making a direct comparison between calculated values and experimental data, we report an example to show how the proposed approach works. In particular, we consider a hydrophilic tubular membrane with an inner diameter equal to 9.3 mm and smooth surface. The membrane pores have a slot shape, while their sizes range from 0.5 to 10 μm. The used interfacial tension and the cross-flow velocity are 7 mN/m and 1.4 m/s, respectively. Although the considered cross-flow velocity is related to a turbulent continuous flow (Reynolds number 13020), in the boundary layer at very short distances from the membrane surface, the continuous flow can be considered laminar. In particular, the following equation is used to obtain the shear stress (at the membrane surface) from the average cross-flow velocity ($\langle v\rangle_c$) of continuous phase, flowing in the membrane tube with D_i inner diameter [12]:

$$\tau_{c,s} = 0.0395 \frac{\mu_c^{0.25} \rho_c^{0.75} \langle v\rangle_c^{1.75}}{D_i^{0.25}}. \quad (8)$$

Table 1 reports the minimum and maximum (Max1, Max2) droplet diameters obtained by using Eq. (3), with process and membrane parameters above considered. Starting from the pore size value (D_p), we change the $\langle D_{droplet}\rangle$ value in Eq. (3) until we find real solutions of the equations. For pores with slot shaped contact lines and sizes below 8 μm, the sets of solutions are not continuous, as shown in Fig. 3. In particular, the $\langle D^{Min1}_{droplet}\rangle$ and $\langle D^{Max1}_{droplet}\rangle$

values represent the interval limits, in which each $\langle D_{\text{droplet}}\rangle$ value is a real solution of Eq. (3), whereas every $\langle D_{\text{droplet}}\rangle$ value in the interval $[\langle D^{\text{Max1}}_{\text{droplet}}\rangle, \langle D^{\text{Min2}}_{\text{droplet}}\rangle]$ is not a real solution of equations. The $\langle D_{\text{droplet}}\rangle$ diameters in the last range $[\langle D^{\text{Min2}}_{\text{droplet}}\rangle, \langle D^{\text{Max2}}_{\text{droplet}}\rangle]$ are again solutions of Eq. (3). In other terms, for droplet diameters in the set $[\langle D^{\text{Max1}}_{\text{droplet}}\rangle, \langle D^{\text{Min2}}_{\text{droplet}}\rangle]$ or bigger than $\langle D^{\text{Max2}}_{\text{droplet}}\rangle$ no advancing and receding contact angles with physical meaning (see following) exists; i.e., no force balance along the contact line can be admitted. The minimum droplet diameters $\langle D^{\text{Min1}}_{\text{droplet}}\rangle$ are obtained by means of Eq. (3) when the first advancing and receding contact angles, having physical meaning (see following), are found. On the contrary, the $\langle D^{\text{Max2}}_{\text{droplet}}\rangle$ diameters are obtained when the last advancing and receding contact angles, having physical meaning, are found.

In Fig. 3 we illustrate the two types of solution sets. For a contact line having slot shape (Fig. 3a) no force balance exists along contact line in the range $[\langle D_{\text{droplet}}\rangle = D_{\text{p}}, \langle D^{\text{Min1}}_{\text{droplet}}\rangle]$. This set can be due to the particular subdivision of the contact line employed (see Appendix A). In the following interval, i.e. $[\langle D^{\text{Min1}}_{\text{droplet}}\rangle, \langle D^{\text{Max1}}_{\text{droplet}}\rangle]$, the force balance exists with both receding and advancing contact angles bigger than $\pi/2$ (physical meaning), since we have considered a hydrophilic membrane together with the oil and water phases. In the range $[\langle D^{\text{Max1}}_{\text{droplet}}\rangle, \langle D^{\text{Min2}}_{\text{droplet}}\rangle]$ and for pore sizes lower than 8 μm, no solution of Eq. (3) exists. Finally, for droplet diameter in the set $[\langle D^{\text{Min2}}_{\text{droplet}}\rangle, \langle D^{\text{Max2}}_{\text{droplet}}\rangle]$, Eq. (3) gives again solution with the receding contact angle smaller than $\pi/2$ and the advancing contact angle bigger than $\pi/2$. Therefore, we found that for $\langle D^{\text{Max1}}_{\text{droplet}}\rangle$ limit the receding contact angle is larger than $\pi/2$, whereas it is lower than $\pi/2$ for droplet diameter ranging between $\langle D^{\text{Min2}}_{\text{droplet}}\rangle$ and $\langle D^{\text{Max2}}_{\text{droplet}}\rangle$. On the contrary, this behaviour was not found for advancing contact angle, which is always bigger than $\pi/2$. For the circular contact line (Fig. 3b), the $\langle D^{\text{Min1}}_{\text{droplet}}\rangle$ limit disappears, while in the first interval $[\langle D_{\text{droplet}}\rangle = D_{\text{p}}, \langle D^{\text{Max1}}_{\text{droplet}}\rangle]$ (except D_{p}) the force balance along the contact line exists. Like slot pores, in the set $[\langle D^{\text{Max1}}_{\text{droplet}}\rangle, \langle D^{\text{Min2}}_{\text{droplet}}\rangle]$, the force balance does not exist whereas in the last set $[\langle D^{\text{Min2}}_{\text{droplet}}\rangle, \langle D^{\text{Max2}}_{\text{droplet}}\rangle]$ exists. The contact angles, evaluated at the limits of these intervals, present the same behaviour as described above for the slot shape case.

From the analysis of the receding contact angles, we could define two conditions for droplet formation: the droplet detachment may occur in the interval $[\langle D^{\text{Max1}}_{\text{droplet}}\rangle, \langle D^{\text{Max2}}_{\text{droplet}}\rangle]$ when the receding contact angle becomes smaller than $\pi/2$ (see Figs. 3 and 4), or in the $[\langle D^{\text{Min1}}_{\text{droplet}}\rangle, \langle D^{\text{Max2}}_{\text{droplet}}\rangle]$ range in which the droplet may not be bent on the membrane surface. The first condition permits to establish the range where the droplet diameter should fall, whereas the second (less restrictive) only permits to define the maximum droplet size above which the force balance along droplet contact line does not exist, $D^{\text{Max2}}_{\text{droplet}}$. Although a dynamic study of droplet detachment should provide a theoretical validation of these conditions, the comparison between the calculated $(D^{\text{Max1}}_{\text{droplet}}/D_{\text{p}})$ and $(D^{\text{Max2}}_{\text{droplet}}/D_{\text{p}})$ with the experimental data shows that these assumptions can be admitted. However, the droplet formation with diameter lower than $\langle D^{\text{Max2}}_{\text{droplet}}\rangle$ can occur by means of a detachment mechanism in which the interface free energy minimization is the driving force.

To clarify the previous important assumptions, in Fig. 4 we present the receding and advancing contact angles corresponding to membrane pore diameters of 0.5, 1.0, 2.0, 6.0 and 10.0 μm, respectively and obtained by using slot shaped contact lines. For pore sizes equal to 0.5 μm (Fig. 4a) the first real solution of Eq. (3) ($\langle D^{\text{Min1}}_{\text{droplet}}\rangle$) corresponds to droplet diameters equal to 0.7 μm with θ_{receding} (triangles) and $\theta_{\text{advancing}}$ (squares) equal to 100.6° and 101.2°, respectively. These angles are larger than 90° because we have considered a hydrophilic membrane. This figure shows that θ_{receding} and $\theta_{\text{advancing}}$ increase in an asymmetric way until $\langle D^{\text{Max1}}_{\text{droplet}}\rangle$. After which no solutions of Eq. (3) are found until $\langle D^{\text{Max2}}_{\text{droplet}}\rangle$ (dashed line), for which θ_{receding} completely changes its value (11.06°), whereas $\theta_{\text{advancing}}$ is almost the same as the previous one (178.0°). For pore sizes ranging from 0.5 to 6.0 μm, we find the same trend in terms of contact angles. On the contrary, for pore size ranging from 8 to 10 μm, the $\langle D^{\text{Max1}}_{\text{droplet}}\rangle$ limits disappear and solution sets become continuous (Fig. 4e). However, the variation of θ_{receding} and $\theta_{\text{advancing}}$ remains similar to the previous calculations. These results show that the droplet grows asymmetrically with both contact angles larger than 90° until the θ_{receding} reaches a maximum value. After this value, the θ_{receding} angles quickly become smaller than 90° in no equilibrium or equilibrium way (in terms of force balance), according to membrane pore sizes. On the contrary, the $\theta_{\text{advancing}}$ always remains over 90°. Therefore, we can conclude that droplets with diameters ranging in the $[\langle D^{\text{Min1}}_{\text{droplet}}\rangle, \langle D^{\text{Max1}}_{\text{droplet}}\rangle]$ interval (when this interval exists) are not bent on the membrane surface, whereas droplets with diameters equal or bigger than $\langle D^{\text{Min2}}_{\text{droplet}}\rangle$ are bent on the membrane surface. Concerning this last point, it is important to stress that for pore sizes ranging from 8 to 10 μm, the sets of solutions are continuous, therefore $\langle D^{\text{Max1}}_{\text{droplet}}\rangle$ does not exist. In these cases, this limit corresponds to the value when the receding contact angle becomes lower than 90°, as shown in Fig. 4e (vertical line).

These results can be useful to evaluate the slopes of the linear correlation between the droplet and pore sizes. In the last two columns of Table 1, we report the ratios $\langle D^{\text{Max1}}/D_{\text{droplet}}\rangle/D_{\text{p}}$, and $\langle D^{\text{Max2}}_{\text{droplet}}\rangle/D_{\text{p}}$, respectively. It is interesting to note that the ratio between $\langle D^{\text{Min}}_{\text{droplet}}\rangle$ and D_{p} is always 1.4, independently from the pore dimensions. If the experimental linear correlation is admitted, the last column of Table 1 shows that for pore sizes ranging from 0.5 to 10 μm, slopes larger than 4.45 are not in agreement with the force balance made on the considered contact line. If we consider that droplet detachments can occur when the droplet sizes fall within the whole interval, i.e. $\langle D^{\text{Min1}}_{\text{droplet}}\rangle$ and

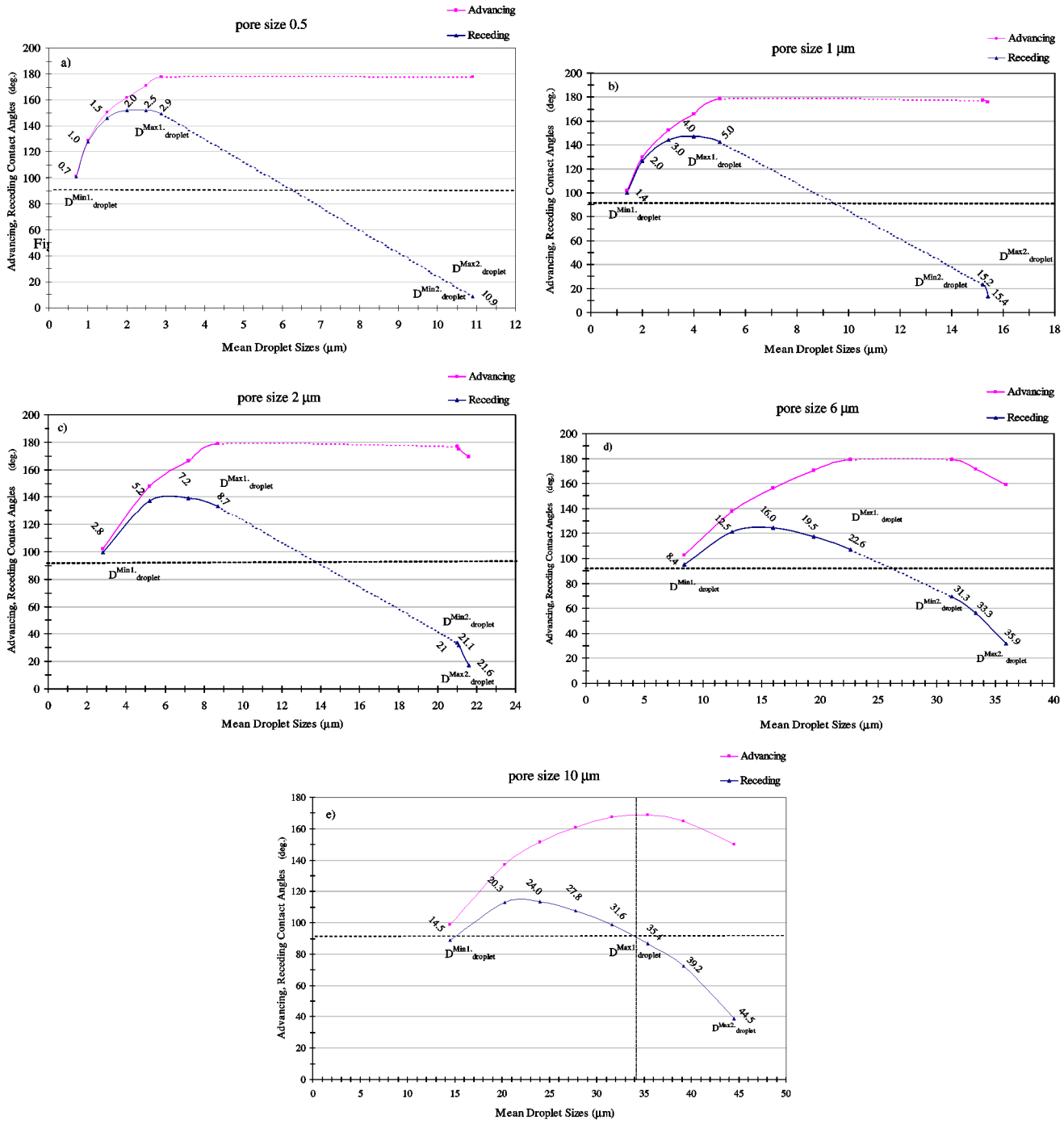

Fig. 4. Receding and advancing contact angles according to Eq. (3) for a slot shaped contact line using interfacial tension and continuous cross-flow velocity equal to 7 mN/m and 1.4 m/s, respectively. The membrane pore diameter is 0.5 (a), 1.0 (b), 2.0 (c), 6.0 (d) and 10 µm (e). The dashed line indicates that Eq. (3) have no real solution in the droplet size range.

$\langle D_{\text{droplet}}^{\text{Max2}} \rangle$ (when the droplet may not be bent on the membrane surface, second condition), then the slopes of the linear correlation between droplet and pore sizes must fall in the interval [1.4, 4.45]. If we consider that droplet detachment occurs when droplet is bent on the membrane surface, in the same direction of cross-flow, (i.e., with $\langle D_{\text{droplet}} \rangle$ within $\langle D_{\text{droplet}}^{\text{Max1}} \rangle$ and $\langle D_{\text{droplet}}^{\text{Max2}} \rangle$, first condition) then for pore sizes between 2.0 and 10 µm the larger slope for the linear correlation in agreement with the force balance is 4.45, but for pore sizes between 0.5 and 1.0 µm this slope is not valid. Fig. 5 shows the correlation between $\langle D_{\text{droplet}}^{\text{Max1}} \rangle / D_{\text{p}}$ (triangles, dashed line), $\langle D_{\text{droplet}}^{\text{Max2}} \rangle / D_{\text{p}}$ (squares) and pore sizes. From Fig. 5, it is clear that if we increase the pore size, the $\langle D_{\text{droplet}}^{\text{Max1}} \rangle / D_{\text{p}}$ and $\langle D_{\text{droplet}}^{\text{Max2}} \rangle / D_{\text{p}}$ ratios decrease, with different rapidity, to an "asymptotic" limit. Therefore, for large pore size intervals, a single slope for the linear corre-

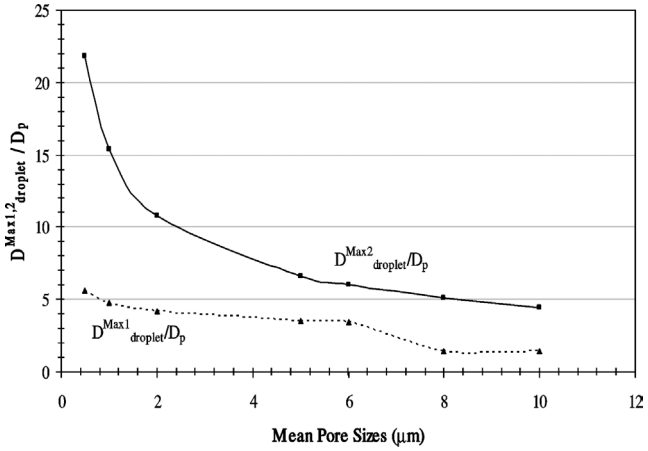

Fig. 5. Correlation between $D^{\mathrm{Max1}}_{\mathrm{droplet}}/D_{\mathrm{p}}$ (▲, - - -), $D^{\mathrm{Max2}}_{\mathrm{droplet}}/D_{\mathrm{p}}$ (■, —) and pore sizes. The maximum droplet diameters (Max1 and Max2) are obtained by means of Eq. (3) using contact line having slot shape.

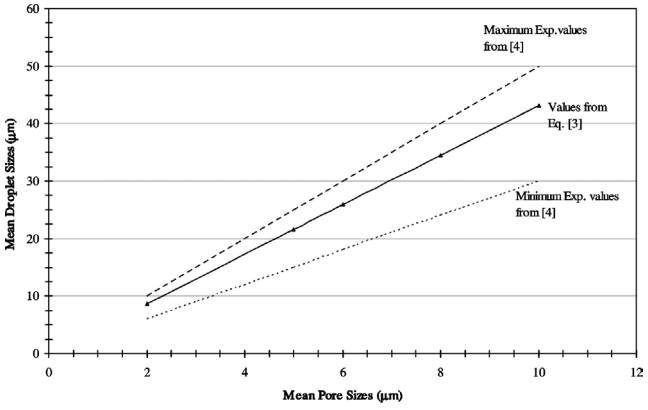

Fig. 6. Correlation between droplet size and mean pore size. The dashed lines indicate the maximum and minimum experimental values, as reported in the review of Joscelyne and Trägårdh [4], for process parameters and membranes similar to those used in the present calculations. The continuous line (▲) represents the calculated values, using 4.45 as slope for the linear correlation between pore size and droplet size and assuming a slot shaped contact line.

lation between droplet and pore size may be incorrect. The analysis of force balance, along the considered contact line, would show that if the droplet detachment only occurs when the droplet is bent on the membrane surface, i.e., when the droplet size is within $\langle D^{\mathrm{Max1}}_{\mathrm{droplet}}\rangle$ and $\langle D^{\mathrm{Max2}}_{\mathrm{droplet}}\rangle$ range, then two slopes should be admitted in the [0.5, 10] pore size interval.

To compare the calculated and the experimental droplet sizes, it is important to consider the fraction of droplet volume that remains attached to the pore border. If we use 4.45 as the slope for the linear correlation between droplet and pore sizes then the experimental droplet diameters will be smaller than the calculated values. However, these experimental droplets cannot be very different from the theoretical ones, since the fraction of attached volume at the pore border must be small compared to the total droplet volume. Joscelyne and Trägårdh [4], in their review about cross-flow membrane emulsification, have reported that several oil-in-water emulsions are produced with average droplet sizes between 3 and 5 times the nominal pore diameter of hydrophilic no pre-treated membranes. Although, in our calculations, we consider a general system, the slope of 4.45 is in agreement with experimental slopes reported by Joscelyne and Trägårdh, as shown in Fig. 6.

Table 2
Maximum (Max1 and Max2) droplet diameters according to Eq. (3) using circular contact line and pore sizes ranging from 0.4 to 10.0 µm. The employed interfacial tension and cross-flow velocity are equal to 7 mN/m and 1.4 m/s, respectively. The experimental pore sizes are taken from Vladisavljevic and Schubert [7] and refer to SPG tubular membranes

Exp. pore size, D_{p} (µm)[a]	$\langle D^{\mathrm{Max1}}_{\mathrm{droplet}}\rangle$ (µm)	$\langle D^{\mathrm{Max2}}_{\mathrm{droplet}}\rangle$ (µm)	$D^{\mathrm{Max1}}_{\mathrm{droplet}}/D_{\mathrm{p}}$	$D^{\mathrm{Max2}}_{\mathrm{droplet}}/D_{\mathrm{p}}$
0.4	2.1	12.2	5.25	30.50
1.4	5.7	22.6	4.07	16.14
2.5	8.9	29.9	3.56	11.96
5.0	15.4	41.3	3.08	8.26
6.6	19.4	46.8	2.94	7.09
10.0	27.6	56.0	2.76	5.60

[a] The last pore size is not taken from Vladisavljevic and Schubert [7].

On this basis, we have repeated the same calculations using experimental pore sizes and a circular contact line shape. Table 2 reports the results of calculations applied to pore sizes used in the work of Vladisavljevic and Schubert [7]. They used Tween 80 emulsifier to produce oil-in-water emulsions at a cross-flow velocity equal to 1.4 m/s. Concerning the choice of the γ value, attention must be paid to the reliability of the dynamic interfacial tension measured with the bursting membrane method, since the timescale of the bursting method may not correspond exactly to the age of the interface (oil/water) during the droplet formation in cross-flow membrane emulsification [11]. Therefore, we have repeated the calculations with the same interfacial tension value of 7 mN/m, which can be considered as the lower limit of the dynamic interfacial tension with Tween 80 [21]. However, in contrast with the previous calculations, in this case we use a circular contact line with a diameter equal to the experimental pore size.

We find that the slopes for a linear correlation between droplet and pore diameters must fall (according to the first condition) in the interval [5.25, 5.60], for pore sizes ranging from 0.4 to 10.0 µm. If we consider the upper limit (5.60), the agreement between experimental and theoretical slopes is not satisfactory; in fact the experimental slope is equal to 3.5. This disagreement can be mainly due to the shape of the contact line, the direction of **m** vector, and/or a different droplet detachment mechanism, in which the driving force is not the cross-flow of continuous phase but the interface free energy minimization. Concerning these points, it is important to note that for circular contact lines, the $\langle D^{\mathrm{Min1}}_{\mathrm{droplet}}\rangle$ lower limit does not exist (Fig. 3b). Therefore, if we consider that the droplet detachment occurs when droplet size falls in the range $[\langle D^{\mathrm{Max1}}_{\mathrm{droplet}}\rangle, \langle D^{\mathrm{Max2}}_{\mathrm{droplet}}\rangle]$, i.e., when the receding contact angle ($\theta_{\mathrm{receding}}$) becomes smaller than 90°, then the value of

Table 3
Maximum (Max1 and Max2) droplet diameters (in micron) according to balance equation (3) using a circular and slot contact line and pore sizes between 0.57 and 10.0 μm. The used interfacial tension and average cross-flow velocity are equal to 4 mN/m and 0.61 m/s, respectively. The experimental data are taken from Katoh et al. [6] and refer to SPG tubular membranes

Exp. pore size, D_p (μm)	$\langle D^{Max1}_{droplet} \rangle$	$\langle D^{Max2}_{droplet} \rangle$	$\langle D^{Max2}_{droplet} \rangle$ (slot)	$D^{Max1}_{droplet}/D_p$	$D^{Max2}_{droplet}/D_p$	$D^{Max2}_{droplet}/D_p$ (slot)	$D^{Exp.}_{droplet}$
0.57	3.57	22.87	18.29	6.26	40.12	32.09	2.85
1.10	5.80	31.70	25.37	5.27	28.82	23.06	5.50
2.34	10.44	45.80	36.80	4.46	19.57	15.73	11.70
10.00	32.40	91.30	73.30	3.24	9.13	7.33	n.a.[a]

[a] n.a.: not available.

Table 4
Maximum (Max1 and Max2) droplet diameters (in micron) according to balance equation (3) using a circular and slot contact line and pore sizes between 0.57 and 10.0 μm. The used interfacial tension and average cross-flow velocity are equal to 4 mN/m and 0.90 m/s, respectively. The experimental data are taken from Katoh et al. [6] and refer to SPG tubular membranes

Exp. pore size, D_p (μm)	$\langle D^{Max1}_{droplet} \rangle$	$\langle D^{Max2}_{droplet} \rangle$	$\langle D^{Max2}_{droplet} \rangle$ (slot)	$D^{Max1}_{droplet}/D_p$	$D^{Max2}_{droplet}/D_p$	$D^{Max2}_{droplet}/D_p$ (slot)	$D^{Exp.}_{droplet}$
0.57	2.97	16.07	13.01	5.21	28.19	22.82	2.85
1.10	4.90	22.30	18.00	4.45	20.27	16.36	5.50
2.34	8.84	32.24	26.10	3.78	13.78	11.15	11.70
10.00	28.10	63.60	51.20	2.81	6.36	5.12	n.a.[a]

[a] n.a.: not available.

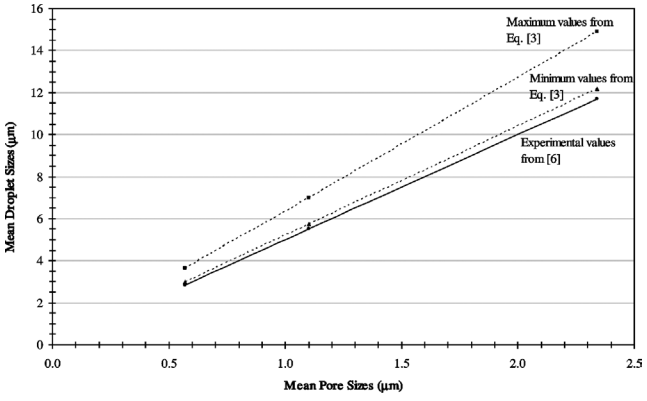

Fig. 7. Correlation between droplet size and mean pore size. The dashed lines indicate the maximum and minimum droplet diameters according to Eq. (3) (using circular contact line), while the experimental values are taken from the work of Katoh et al. [6] (continuous line and circle points) and refer to SPG tubular membrane emulsifications.

5.25 can be considered as a lower limit. If the droplet detachment can occur when both receding and advancing contact angles are larger than 90°, then the slope could be smaller than 5.25. Taking into account the fraction of droplet volume that remains attached to the pore border, it is interesting to note that if the value of 4.45 (found for a contact line with a slot shape) would be used, the agreement with the experimental results is satisfactory. This consideration shows how the proper choice of contact line shape and direction of **m** vector are particularly important in this method.

Katoh et al. [6] have used the same tubular SPG membrane to produce oil-in-water emulsions, but they employed different surfactants, sucrose esters, polyglycerol esters and above all sodium dodecyl sulphate (SDS). The SDS lowers the interfacial tension of droplet very quickly to a constant value of 4 mN/m. The cross-flow velocities used by Katoh et al. [6] are smaller than velocity employed by Vladisavljevic and Schubert [7], thus they should obtain larger droplet diameters than Vladisavljevic and Schubert's. In Tables 3 and 4, we report the results obtained by balance equation (3), using a circular and slot contact line, pore sizes (the first three values) and experimental parameters (cross-flow velocities, interfacial tension) taken from Katoh et al [6]. The results of Table 4 (D^{Max2}/D_p) are in agreement with the experimental slope value. In fact, the experimental slope of the linear correlation between droplet size and pore size is equal to 5.0 with a correlation coefficient equal to 0.99. Fig. 7 shows that the theoretical slopes fall within the interval [5.21, 6, 36], if the first condition for droplet detachment is considered. Moreover, if the same calculations, presented in Table 4 (D^{Max2}/D_p (slot)), are repeated with contact line having a slot shape, we obtain an upper slope of 5.12. It is important to consider that the last pore size, in Tables 3 and 4 (10 μm), is necessary to find the quoted "asymptotic" limit (Fig. 5).

The results of Tables 3 and 4 show that the droplet detachment could occur in the equilibrium range $[D_p, \langle D^{Max1}_{droplet} \rangle]$ by means of a detachment mechanism (not according to the force balance conditions), in which the driving force is the interface free energy minimization. In fact, depending on the cross-flow velocity, the balance equation (3) yields results in agreement (see Table 4) or not (see Table 3) with experimental data.

In this context, Kobayashi et al. [20] have reported the influence of the continuous phase flow velocity and surfactant type (Tween 20 and SDS) on the droplet diameter, during a membrane emulsification process. Unlike the SPG membrane, the pore shapes of polycarbonate membranes are circular with well defined diameters; therefore a circular shape of contact line becomes more realistic.

Table 5
Maximum (Max1 and Max2) droplet diameters according to Eq. (3) using a circular contact line. The used interfacial tensions ranging from 1.0 to 10.0 mN/m, while the membrane pore size is 10 μm. The experimental mean droplet diameters, obtained using Tween 20 emulsifier, are taken from Kobayshi et al. [20] and refer to flat rectangular polycarbonate membranes

Average cross-flow velocity (m/s)		Interfacial tension (mN/m)										$\langle D^{\text{Exp}}_{\text{droplet}} \rangle$ (μm)
		1.0	**2.0**	3.0	**4.0**	5.0	6.0	7.0	8.0	9.0	10.0	
0.27	$\langle D^{\text{Max1}}_{\text{droplet}} \rangle$	22.4	24.6	26.7	28.4	29.8	31.1	32.2	33.2	34.1	35.0	∼ 60.5
	$\langle D^{\text{Max2}}_{\text{droplet}} \rangle$	32.7	46.6	56.9	**65.4**	72.8	79.3	85.2	90.7	95.7	100.4	
0.35	$\langle D^{\text{Max1}}_{\text{droplet}} \rangle$	28.4	23.9	25.5	27.1	28.3	29.5	30.5	31.4	32.3	33.1	∼ 27.1
	$\langle D^{\text{Max2}}_{\text{droplet}} \rangle$	28.4	40.6	49.7	57.1	**63.6**	69.1	74.5	79.3	83.7	87.8	
0.44	$\langle D^{\text{Max1}}_{\text{droplet}} \rangle$	24.9	23.4	24.6	25.9	27.1	28.1	29.1	30.0	30.8	31.5	∼ 20.0
	$\langle D^{\text{Max2}}_{\text{droplet}} \rangle$	24.9	35.9	44.0	50.7	56.4	**61.5**	66.2	70.4	74.4	78.0	
0.53	$\langle D^{\text{Max1}}_{\text{droplet}} \rangle$	22.3	24.1	24.3	25.4	26.4	27.4	28.3	29.1	29.9	30.5	∼ 20.0
	$\langle D^{\text{Max2}}_{\text{droplet}} \rangle$	22.3	32.4	39.8	45.9	51.2	55.8	**60.1**	63.9	67.5	70.9	
0.63	–	20.0	29.5	24.2	24.9	25.8	26.7	27.5	28.3	29.1	29.6	∼ 20.0
	$\langle D^{\text{Max2}}_{\text{droplet}} \rangle$	20.0	29.5	36.3	41.9	46.7	51.0	54.8	58.4	**61.7**	64.7	

Using the following relation (Schröder et al. [11]), the mean droplet formation time can be evaluated:

$$t_f = \frac{2}{3}\frac{\varepsilon k}{D_p^2}\frac{\langle D_{\text{droplet}} \rangle^3}{J_d}, \tag{9}$$

where ε is the membrane porosity, k is the ratio between active pores and total number of membrane pores and J_d is the disperse phase flux. From experimental disperse phase flux, reported by Kobayashi et al. [18] (137 l/(m^2 h)), we have calculated by means of Eq. (9) the mean formation time of droplets with diameters of 28.2 μm, which are obtained using 0.3 wt% of SDS and a cross-flow velocity equal to 0.18 m/s. The average droplet formation time is equal to 1 ms. Afterwards, using the experimental dynamic interfacial tension of SDS (reported in the paper of Schröder et al. [11]) and the found droplet formation time, we have evaluated the corresponding value of interfacial tension at the droplet formation time [13]. The obtained value is too high respect to the interfacial tension reported by the Kobayashi et al. in their paper. Also with Tween 20 and the corresponding experimental disperse phase flux, the interfacial tension obtained by means of the dynamic interfacial tension function is higher than that reported in the Kobayashi et al. paper.

On this basis, in Table 5 we calculate the maximum (Max1 and Max2) droplet diameters by using Eq. (3), with interfacial tensions ranging from 1 to 10 mN/m. The cross-flow velocities are those used by Kobayashi et al., while the equation used to obtain the corresponding shear stress is:

$$\tau_{c,s} = 6\frac{\mu_c \langle v \rangle_c}{D}, \tag{10}$$

where D represents the thickness of the continuous phase fluid film above the membrane surface.

In the last column of Table 5, we report the experimental droplet diameters obtained using Tween 20 surfactant. The experimental droplet sizes, using SDS as the emulsifier, were almost equal to 20 μm for all considered cross-flow velocities. From an analysis of these results it has emerged that for cross-flow velocity equal to 0.27 m/s, interfacial tensions lower than 4 mN/m should not be admitted (when Tween 20 is used), since the $\langle D^{\text{Max2}}_{\text{droplet}} \rangle$ droplet diameters obtained using interfacial tensions lower than this value are always smaller than the experimental droplet size (60.5). For a cross-flow velocity above 0.27 m/s the lower limit of interfacial tension becomes larger (see the corresponding bold values in Table 5). If we suppose that the adsorption rate of the surfactant during droplet formation does not depend on the cross-flow velocity, then for Tween 20 the interfacial tension in agreement with all the experimental droplet sizes should be 4.0 mN/m. Kobayashi et al. obtained a constant droplet diameter almost equal to 20 μm using SDS emulsifier for all considered cross-flow velocity. In this case, the interfacial tension in agreement with experimental droplet size is 2.0 mN/m (see Table 5). In fact, interfacial tensions bigger than 2.0 mN/m would yield large attached oil volumes on the contact line (>20%) and therefore these interfacial tensions are less probable. It is interesting to note that for interfacial tensions equal to 1 mN/m and cross-flow velocities larger than 0.27 m/s the $\langle D^{\text{Max1}}_{\text{droplet}} \rangle$ limit disappears, while the receding contact angles slowly change but not as quickly as found for the other interfacial tensions.

The interfacial tensions obtained from analysis of the solutions of Eq. (3) (i.e., 2.0 and 4.0 mN/m) and considering circular contact line, are approaching the interfacial tensions presented in the paper of Kobayashi et al. but do not correspond to the values obtained using the experimental dynamic interfacial tension functions. Taking into account the problem concerning the timescale in the measurement of the dynamic interfacial tension by using the membrane bursting method, these last calculations show that, when the droplet

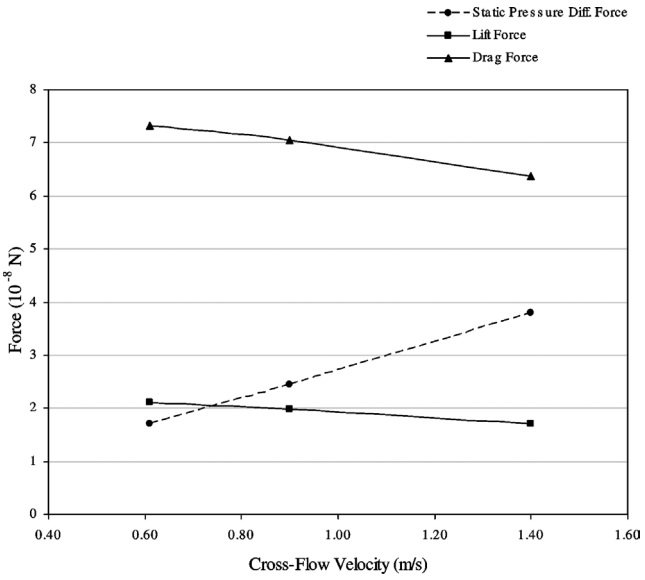

Fig. 8. Correlation between the forces used in Eq. (3) and cross-flow velocity. The calculated values are obtained using pore size equal to 10 µm (slot section and tubular membrane), interfacial tension equal to 4 mN/m and cross-flow velocities equal to 0.61, 0.90, 1.4 m/s. The force contributions are evaluated by using droplet sizes equal to $D^{\mathrm{Max2}}_{\mathrm{droplet}}$ diameters.

sizes are well known, the balance equation (3) could be also used to evaluate the interfacial tension during the droplet formation. Moreover, if the length of the integrations in Eq. (3) is considered equal to the membrane pore size (see Appendix A) it is possible to obtain droplet diameters close to the Kobayashi et al. [20] values.

Finally, in Fig. 8, we report the influence of cross-flow velocity on the forces which define Eqs. (1) and (3). Fig. 8 refers to results obtained by using membrane pore size equal to 10 µm with slot section (tubular membrane), interfacial tension equal to 4 mN/m and cross-flow velocities equal to 0.61, 0.90 and 1.4 m/s, respectively. It is important to emphasize that the forces of Fig. 8 are evaluated using droplet sizes equal to the corresponding $\langle D^{\mathrm{Max2}}_{\mathrm{droplet}}\rangle$ diameters. Fig. 8 shows that the drag force (F_{DR}) is the larger force. Moreover, the F_{DR} and the lift force (F_{DL}) decrease with the increase of the cross-flow velocity, whereas the static pressure difference force (F_{YL}) increases. The F_{DR} and F_{DL} forces depend on $\langle D_{\mathrm{droplet}}\rangle^2$ and $\langle D_{\mathrm{droplet}}\rangle^3$, respectively (see Eqs. (7) and (5)), whereas they depend on cross-flow velocity according to $\langle v\rangle_{\mathrm{c}}^{1.75}$ and $\langle v\rangle_{\mathrm{c}}^{2.6}$. Increasing the $\langle v\rangle_{\mathrm{c}}$ variable the $\langle D^{\mathrm{Max2}}_{\mathrm{droplet}}\rangle$ decreases, consequently the F_{DR} and F_{DL} forces decrease also. On the contrary (according to Fig. 8), the F_{YL} force increases with the cross-flow velocity, because this force is inverse proportional to $\langle D_{\mathrm{droplet}}\rangle$ (see Eq. (4)) and does not depend on the $\langle v\rangle_{\mathrm{c}}$. Therefore, the decrease of $\langle D^{\mathrm{Max2}}_{\mathrm{droplet}}\rangle$ with the cross-flow velocity causes an increase of F_{YL} force. We find that the $\langle D^{\mathrm{Max2}}_{\mathrm{droplet}}\rangle$ decreases with cross-flow velocity not linearly but with a behaviour similar to the one reported in Fig. 5. Naturally, if the same calculations are repeated with a $\langle D_{\mathrm{droplet}}\rangle$ constant then both F_{DR} and F_{DL} increase with the cross-flow, whereas F_{YL} remains constant. Finally, the values of the buoyancy force F_{BG} are two orders of magnitude smaller than the forces reported in Fig. 8.

4. Summary

Although droplet formation in a membrane emulsification process can be described using computational fluid dynamics or theoretical methods based on interface free energy minimization rather than force approaches, these latter are easier to handle and instructive. Therefore, the aim of this work was to test the reliability of new balance force equations, based on the evaluation of receding and advancing contact angles along the droplet contact line.

We propose a force balance made along the droplet contact line, located on the membrane surface around the pore borders. Using two contact line shapes (slot and circular), a quantitative description of maximum sizes that the droplets, stuck on the pore border, could have are presented.

The analysis of receding and advancing contact angles allows a better understanding of the droplet detachment mechanisms during cross-flow membrane emulsification. Aware that different mechanisms can occur during this process, in this work the cases in which the continuous phase cross-flow has an important role in the droplet detachment have been considered.

We suggest also two conditions for droplet formation: the droplet detachment may occur in the interval $[\langle D^{\mathrm{Max1}}_{\mathrm{droplet}}\rangle, \langle D^{\mathrm{Max2}}_{\mathrm{droplet}}\rangle]$ when the receding contact angle ($\theta_{\mathrm{receding}}$) becomes smaller than 90° (see Fig. 4e), or in the $[\langle D^{\mathrm{Min1}}_{\mathrm{droplet}}\rangle, \langle D^{\mathrm{Max2}}_{\mathrm{droplet}}\rangle]$ range in which the droplet may not be bent on the membrane surface. The first condition permits to define the lower ($\langle D^{\mathrm{Max1}}_{\mathrm{droplet}}\rangle$) and upper $\langle D^{\mathrm{Max2}}_{\mathrm{droplet}}\rangle$ limits in which the droplet diameter should fall, whereas the second (less restrictive) permits to define only a maximum droplet size. The comparison between calculated ($D^{\mathrm{Max1}}_{\mathrm{droplet}}/D_{\mathrm{p}}$) and ($D^{\mathrm{Max2}}_{\mathrm{droplet}}/D_{\mathrm{p}}$) with experimental slopes of the linear correlation between droplet and pore sizes shows that these assumptions may be admitted. However, in this work it has been assumed that the linear correlation between droplet and pore sizes goes through the origin, otherwise the suggested conditions can not be used. One of the aims of the work is to define a maximum droplet diameter, i.e. $\langle D^{\mathrm{Max2}}_{\mathrm{droplet}}\rangle$ (less restrictive condition), so that droplet with diameter bigger than this value should slide along the membrane surface. As shown in Fig. 5, interesting insights on droplet and pore size correlation can be obtained from relationship between ($D^{\mathrm{Max2}}_{\mathrm{droplet}}/D_{\mathrm{p}}$) and membrane pores. In fact, the behaviour of ($D^{\mathrm{Max2}}_{\mathrm{droplet}}/D_{\mathrm{p}}$) in function of D_{p} is not linear and presents an “asymptotic” limit. The “asymptotic” behaviour of ($D^{\mathrm{Max2}}_{\mathrm{droplet}}/D_{\mathrm{p}}$) suggests that if a large set of pore diameters is considered then the ($D^{\mathrm{Max2}}_{\mathrm{droplet}}/D_{\mathrm{p}}$) ratio (corresponding to the last pore diameter of the set) will be the larger slope for

the linear correlation between droplet and pore size, going through the origin. Any spontaneous droplet deformation due to neck formation, inside or outside of the pore (according to the aspect ratio of pore section), must occur with droplet diameter below the maximum limits $D_{\text{droplet}}^{\text{Max2}}$.

To test the proposed conditions (above all the less restrictive) we use a particular mathematical method to solve the force balance equations along the droplet contact line, Eq. (1). In general this approach can not be accurate (e.g., the presence of the non-continuous solution sets). Therefore, to verify the reliability of the suggested conditions, attention must be paid to the mathematical approach used to solve the proposed balance equations (work in progress).

On this basis, some interesting conclusions can be drawn:

(i) to obtain good evaluation of experimental data, it is important to have a satisfactory contact line shape (also symmetric shapes);
(ii) the comparison between experimental and model results can give insights in the kind of droplet detachment mechanism;
(iii) the maximum sizes that a droplet can have during a CME process can be calculated;
(iv) for broad pore size ranges, the use of a single slope for the linear correlation between droplet size and pore size can be in disagreement with the force balance made along a considered contact line.

Starting from these results, the conditions that allow an accurate location of droplet size, in the minimum and maximum limits, can be studied.

Acknowledgment

We greatly appreciated the critical reading of manuscript by Dr. Johannes Carolus Jansen.

Appendix A

The first equation of the system (1) can be considered as a derivation of the equation applied to calculate the inclination (critical angle) of a non-horizontal surface on which a droplet is stuck. A complete derivation of this equation is reported in the work of Dussan and Chow [18]. The component of gravity force, parallel to non-horizontal surface in the work Dussan and Chow, is substituted here by the drag force, F_{DR}. The forces, perpendicular to the surface, are F_{YL}, F_{DL} and F_{BG}, and they are equilibrated by the interfacial tension due to the upper part of the droplet contact line.

The force F_{YL} derives from the Young–Laplace pressure [11,12] (static pressure difference between the inside and outside of the droplet) and in the reference [22] it is derived by using a thermodynamic and mechanical approach. Moreover, the Stokes and lift forces are also reported in several transport phenomenon books and in different papers on cross-flow membrane emulsifications [9].

The terms, in the integral calculus of Eq. (1), represent the infinitesimal forces which permit the droplet to stick on the membrane surface. The integral calculus along the contact line yields therefore a total force. Finally, the subdivision of the integral calculus in four parts and the further simplification of the opposite forces yields Eq. (3).

It is important to note that if the **m** vector is always perpendicular to infinitesimal portion of contact line dl (see Fig. 2) then $\int_{l_r} \bar{m} \cdot i \, \mathrm{d}l$ term is equal to D_{p} for slot (in advancing and receding portions) and circular shaped pores. Therefore, for circular contact line calculations, we consider the direction of **m** vector parallel to drag force F_{DR}; in this case the $\int_{l_r} \bar{m} \cdot i \, \mathrm{d}l$ term is equal to $\pi D_{\text{p}}/2$.

Concerning the slot aspect ratio, we assume that the side lines (bc) are much smaller than advancing and receding portions. How small are these lines (bc)? For j-symmetric droplet contact lines, only the perpendicular force components must be considered in the balance along the (bc) lines; furthermore in the side portions the contact angle is not constant. The length of side lines can be evaluated by means of a self-consistent procedure. In particular, we consider the following force contribution:

$$F_{\text{bc}}^{m} = 2\gamma \int_{\text{b}}^{\text{c}} \sin\theta(l) \, \mathrm{d}l \tag{A.1}$$

with

$$\theta(l) = \theta_{\text{r}} + (\theta_{\text{a}} - \theta_{\text{r}}) \left(\frac{l}{\text{bc}} \right)^{n}. \tag{A.2}$$

In the first cycle ($m = 0$), using Eq. (3) we calculate θ_{a} and θ_{r} angles without the $F_{\text{bc}}^{m=0}$ contribution. We use θ_{a} and θ_{r} values in Eq. (A.2) and therefore in (A.1) to evaluate the $F_{\text{bc}}^{m=1}$ contribution, which we introduce in Eq. (3) (second cycle) to evaluate the new θ_{a} and θ_{r} until the convergence of these angles is obtained. Naturally, when the convergence of θ_{a} and θ_{r} is achieved, we find θ_{a} and θ_{r} and the corresponding $\langle D_{\text{droplet}} \rangle$ value, which is a solution of the balance equation (3). If we assume that the side line length is smaller than advancing and receding portions, then for a particular (bc) line, the $\langle D_{\text{droplet}} \rangle$ at the first cycle will be similar to $\langle D_{\text{droplet}} \rangle$ at the last cycle.

In general, a slot pore section can be described by the Longer slot length (L, corresponding to the advancing and receding portions), the Shorter slot length (S, corresponding to the side lines (bc)) and the slot aspect ratio (L/S) [19]. Using L/S equal to 10 (with n equal to 0.5, 1 and 2, respectively) we find that the contribution of F_{bc}^{m} can be neglected for any pore sizes used in the work. It is important to stress that for different L/S ratios the F_{bc}^{m} contribution influences the $\langle D_{\text{droplet}} \rangle$ value and therefore the final $\langle D_{\text{droplet}}^{\text{Max2}} \rangle$. However, although we have tested the reported results by using both logarithmic and exponential (A.2) functions, the study of the F_{bc}^{m} contribution is in progress.

Appendix B. Notation

D	Thickness of rectangular membrane module (thickness of the continuous phase fluid above the membrane surface)
$\langle D_{\text{droplet}} \rangle$	Mean droplet diameter
D_{p}	Mean membrane pore size
D_{i}	Inner diameter of tubular membrane
$\text{d}l$	Differential line element
$F_{\text{YL}}, F_{\text{DL}}, F_{\text{BG}}, F_{\text{DR}}, F_{\text{bc}}^{\text{m}}$	Static pressure difference force, dynamic lift force, buoyancy forces, drag force, slot side line force
J_{d}	Disperse phase flux
$\mathbf{i}, \mathbf{j}, \mathbf{k}$	Unit basis vectors
$l_{\text{a}}, l_{\text{r}}$	Advancing and receding contact lines
$\mathbf{M}, \mathbf{m}$	Unit vectors
ΔP_{eff}	Effective pressure
$\langle v \rangle_{\text{c}}$	Average cross-flow velocity
$v_{\text{c,c}}^{\infty}$	Undisturbed parallel continuous phase velocity
γ	Interfacial tension
ε	Membrane porosity
μ_{c}	Viscosity of the continuous phase
$\theta_{\text{a}}, \theta_{\text{r}}$	Advancing and receding contact angles
$\rho_{\text{c}}, \Delta\rho$	Density of the continuous phase, density difference between continuous and disperse phase
$\tau_{\text{c,s}}$	Wall shear stress

References

[1] T. Nakashima, M. Shimizu, M. Kukizaki, Key Eng. Mater. 61/62 (1991) 513.
[2] A.J. Gijsbertsen-Abrahamse, A. van der Padt, R.M. Boom, J. Membr. Sci. 230 (2004) 149.
[3] A.J. Gijsbertsen-Abrahamse, R. van Lierop, R.G.M. van der Sman, A. van der Padt, R.M. Boom, J. Membr. Sci. 204 (2002) 125.
[4] S.M. Joscelyne, G. Trägårdh, J. Membr. Sci. 169 (2000) 107.
[5] V. Schröder, H. Schubert, Colloids Surf. A: Physicochem. Eng. Aspects 152 (1999) 103.
[6] R. Katoh, Y. Asano, A. Furuya, S. Kazuyoshi, M. Tomita, J. Membr. Sci. 113 (1996) 131.
[7] G.T. Vladisavljevic, H. Schubert, Desalination 144 (2002) 167.
[8] A.J. Gijsbertsen-Abrahamse, A. van der Padt, R.M. Boom, W.B.C. de Heij, AIChE.J. (2001) 1285.
[9] S.J. Peng, R.A. Williams, Trans. IChemE 76 (1998) 894.
[10] M. Rayner, G. Trägårdh, Desalination 145 (2002) 165.
[11] V. Schröder, O. Behrend, H. Schubert, J. Colloid Interface Sci. 202 (1998) 334.
[12] Z. Wang, S. Wang, S. Volker, H. Schubert, Chin. J. Chem. Eng. 8 (2000) 108.
[13] G. De Luca, A. Sindona, L. Giorno, E. Drioli, J. Membr. Sci. 229 (2004) 199.
[14] I. Kobayashi, M. Nakajima, K. Chun, Y. Kikuchi, H. Fujita, AIChE J. 48 (2002) 1639.
[15] M. Yasumo, M. Nakajima, S. Iwamoto, T. Muryama, S. Sugiura, I. Kobayashi, A. Shono, K. Satoh, J. Membr. Sci. 210 (2002) 29.
[16] M. Rayner, G. Trägårdh, Ch. Trägårdh, P. Dejmek, J. Colloid Interface Sci. 279 (2004) 175.
[17] M.E. O'Neil, Chem. Eng. Sci. 23 (1964) 67.
[18] B. Dussan, R.T.P. Chow, J. Fluid Mech. 137 (1983) 1.
[19] I. Kobayashi, S. Mukataka, M. Nakajima, J. Colloid Interface Sci. 279 (2004) 277.
[20] I. Kobayashi, M. Yasumo, S. Iwamoto, A. Shono, K. Satoh, M. Nakajima, Colloids Surf. A: Physicochem. Eng. Aspects 207 (2002) 185.
[21] S. Tesch, Ch. Gerhards, H. Schubert, J. Food Eng. 54 (2002) 167.
[22] J. Pellicer, V. Garcia-Morales, M.J. Hernandez, Phys. Educ. 35 (2) (2000) 126.